



Experimental study of the ignition temperatures of low-rank coals using TGA under oxygen-deficient conditions

Kunlin Cong^{1,2} · Yanguo Zhang^{1,2} · Yu Gan¹ · Qinghai Li^{1,2} 

Received: 20 November 2017 / Accepted: 12 March 2018 / Published online: 31 March 2018
© Akadémiai Kiadó, Budapest, Hungary 2018

Abstract

The factors affecting the ignition temperatures of two low-rank coals were experimentally studied using thermogravimetric analysis. The experiments were conducted with coal powders of four different particle size distributions. The thermogravimetric analyzer was operated at three heating rates, 10, 20, and 30 °C min⁻¹ and four oxygen concentrations of 3, 6, 9, and 12%. The results showed that the ignition temperature decreased by about 25 °C as the oxygen concentration increased from 3% to 12%. The standard deviation of the activation energy was 16.75% at a conversion degree of less than 0.4, and it decreased to 1.35% at the end of the combustion process. At a heating rate of 10 °C min⁻¹, the ignition temperature increased by about 8 °C as the coal particle size increased by 100 μm. At a heating rate of 30 °C min⁻¹, the effect of the particle size on the ignition temperature was enhanced and the ignition temperature increased to 15 °C.

Keywords Ignition temperature · Low-rank coal · Oxygen-deficient combustion · Coal particle size distribution · Thermogravimetric

Introduction

Recent anthropogenic greenhouse gas (GHG) emissions have caused profound climate change and extreme weather conditions [1–4]. However, the predominant energy resource in China is still coal and this situation will remain for the coming decades [5, 6]. Most of the coal used in the industrial boilers in China is of low quality [2], and Chinese industrial enterprises are facing a great challenge to reduce the energy consumption and air emissions. Retrofitting boilers may be an effective approach to alleviate these challenges [7, 8]. Fluidized bed combustion (FBC) has been considered the best technology for burning low-rank coal owing to its fuel adaptability, high combustion

efficiency, and low air emissions [9, 10]. Circulating fluidized bed (CFB) boilers have been widely used in China. Recently, a low-cost horizontal CFB boiler was developed in China to replace the traditional CFB boilers [11]. The furnace in the horizontal CFB boiler is divided into three chambers arranged horizontally side by side, and the particle size distributions and temperatures in the three chambers are different [12, 13]. Graded fuel feeding with different particle sizes in different chambers can be utilized for higher heat efficiency and lower pollutant emissions. The particle sizes of pulverized coal burning in the CFB boilers are in the range of 10–8000 μm in diameter, and the furnace temperature is about 900 °C [14–16].

The ignition is the starting point of the coal combustion and represents the transition from negligible fuel oxidation to fast oxidation of volatiles and other reactive substances [17, 18]. Understanding the ignition behavior of coal is essential to the design of industrial boilers for coal combustion. The coal ignition temperature is a key parameter of a CFB boiler and determines the type of fuel to achieve stable flames. When coal is fed into a furnace at a temperature that is lower than its ignition temperature, the coal powders cannot burn effectively and the furnace temperature will drop [18, 19]. When the unburned coal particles

✉ Qinghai Li
liqh@tsinghua.edu.cn

¹ Key Laboratory for Thermal Science and Power Engineering of Ministry of Education, Department of Energy and Power Engineering, Tsinghua University, Beijing 100084, People's Republic of China

² Tsinghua University-University of Waterloo Joint Research Center for Micro/Nano Energy & Environment Technology, Tsinghua University, Beijing 100084, People's Republic of China

accumulate in the furnace and reach a certain critical concentration, the furnace temperature will increase suddenly, causing furnace overheating [9]. In practical applications in the industry, the coal ignition temperatures are estimated without theoretical justifications. This leads to great uncertainty in the design and operation of a new boiler.

Thermogravimetric (TG) analysis (TGA) is widely used for the measurement of solid-phase thermal degradation mechanisms, and it can also be used for studying the kinetics of coal combustion and pyrolysis [20–26]. Earlier research has shown that the flow rate of the air and coal mixture, the fuel properties, and the surrounding temperature are important factors affecting the ignition of coal at both low and high heating rates [27–32]. Researchers have measured the coal ignition temperatures by TGA, differential scanning calorimetry (DSC), and derivative thermal analysis (DTA) [33]. TG curves can be used to identify the ignition temperature by intersection and deviation [22]. The ignition temperature is also related to the reactivity of the coal. A higher ignition temperature indicates a lower reaction activity [34]. The activation energy can also be used to evaluate the intensity of a combustion-related chemical reaction by using the pre-exponential factor and a reaction model [35–38]. However, there are very limited studies on coal ignition temperatures in a CFB boiler using the TGA method [39]. Most of the existing papers have focused on specific factors that affect the combustion characteristics of coal particles. By summarizing the actual operating parameters of a coal-fired CFB boiler, we find that the severe fluctuations of the furnace temperature have a serious impact on the efficient and safe operation of the boilers. The main reason for this fluctuation is the difficulty in accurately predicting the ignition temperature of the coal particles.

Therefore, one objective of this study is to evaluate the effects of the oxygen concentration, heating rate, and particle size on the ignition temperature of low-rank coal burned in CFB boilers. A second objective is to provide guidance for the design of a graded particle size fuel-feed system by that can increase boiler efficiency and reduce pollutant emissions by supplying coal particles of different particle sizes to different sections of the furnace.

Materials and methods

Materials

The low-rank coals were obtained from two industrial sites in Dechang City, Sichuan Province, and Chenzhou City, Hunan Province in China. The proximate and ultimate analyses of the coal samples were carried out in the Beijing

Coal Chemistry Branch of the China Coal Research Institute and following the GB/T211-213, T476, and T9227 (China) standards. The results are summarized in Table 1 (DC denotes Sichuan Dechang; CZ denotes Hunan Chenzhou). Based on the volatile contents and calorific values shown in Table 1, the coals are classified as lignite according to the GB/T 5751 (China) standard.

The coal samples were crushed and sieved into four different size bins, 90–110, 200–240, 420–460, and 530–630 μm . All samples were sealed and stored in plastic boxes until they were used. The particle size distributions of the samples were determined using a Mastersizer 2000 laser particle size analyzer (Malvern, UK), and the measurement results of the two samples are shown in Fig. 1. (D [4, 3] indicates the volume-weighted mean diameter); the mean particle sizes were 109.87, 235.74, 450.60, 622.28 μm for the DC coal and 92.38, 207.65, 428.59, 539.23 μm for the CZ coal.

Experiments

The TGA of the coal samples was performed using a NETZSCH STA 449F3 thermal analyzer (Selb, Germany). Figure 2 shows the experimental setup, which comprises a data acquisition system, a heating unit, an electronic balance, and a gas supply system. The maximum temperature of the TGA is 1550 $^{\circ}\text{C}$, and the microbalance sensitivity is $\pm 0.1 \mu\text{g}$. The samples (25 mg ± 1 mg) were heated under atmospheric pressure in a crucible (made of Al_2O_3) at heating rates of 10, 20, and 30 $^{\circ}\text{C min}^{-1}$ from the ambient temperature to 104 $^{\circ}\text{C}$, which was maintained for

Table 1 Proximate and ultimate analyses of samples

Sample	DC	CZ
<i>Proximate analysis/mass%</i>		
Moisture, db	2.86	1.83
Ash, db	43.86	40.27
Volatile matter, daf	44.28	31.43
Fixed carbon, db	30.56	40.44
<i>Ultimate analysis/mass%, db</i>		
C	39.52	48.03
H	2.64	3.09
O (by difference)	8.71	5.47
N	0.74	0.69
S	1.69	0.63
<i>Calorific value/MJ kg⁻¹</i>		
GCV, ad	15.86	19.32
NCV, ad	15.17	18.26

Db dry basis, *daf* dry ash free basis, *ad* air-dried basis, *GCV* gross calorific value, *NCV* net calorific value

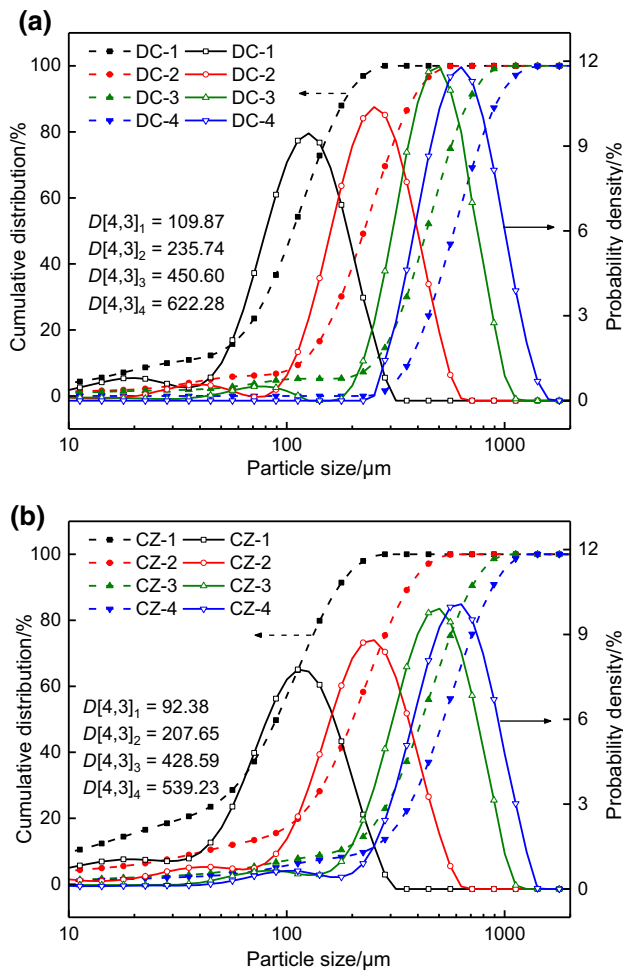
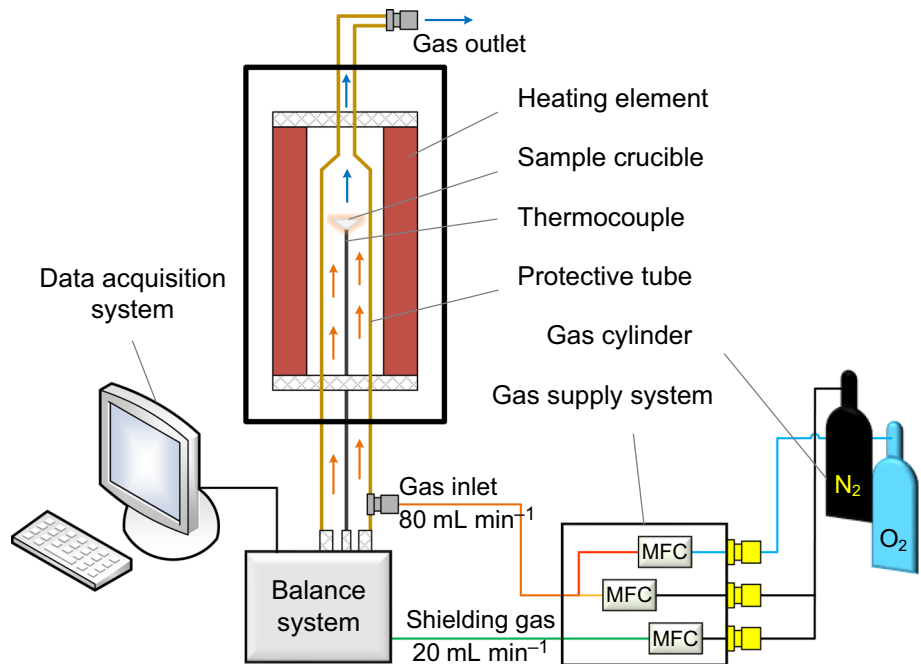


Fig. 1 Particle size distributions of DC coal (a) and CZ coal (b)

Fig. 2 Schematic diagram of experimental setup



30 min. Subsequently, the heating continued until a temperature of 1400 °C was reached. Pure oxygen and nitrogen were employed as the carrier gases in all experiments, and their total flow rates were 100 mL min⁻¹. The inert atmosphere and oxidation atmosphere conditions with 4 different oxygen concentrations (OC) of 3, 6, 9, and 12% were provided by the gas supply system. The stability and precision of the TG analyzer were verified by repeated experiments, which showed that the TG curves had good reproducibility.

A blank TG run was performed with an empty crucible before each test, and the resulting blank TG curve was deducted from the TG curve measured in the presence of a sample in the crucible. Both runs were conducted under identical conditions to minimize the errors caused by the buoyancy force in the vertical furnace.

Figure 3 shows an example of this practice. The black line represents the TG curve for an empty Al_2O_3 crucible (blank), and the red line represents the TG curve of 25.8 mg of the DC (90–110 μm) coal sample (measured). The curves were recorded at a heating rate of 30 °C min⁻¹ with an oxygen concentration of 6%. The difference between these two curves results in the corrected TG curve (blue line). The corrected curve was obtained by deducting the blank curve from the measured curve.

Characterization and kinetic method

The TG and differential TG (DTG) curves obtained as the functions of temperature and time were used to determine

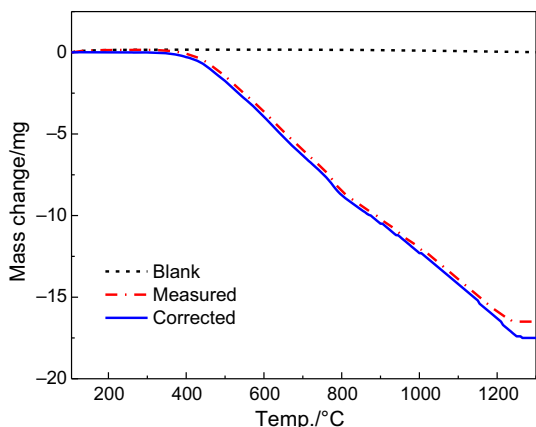


Fig. 3 An example of obtaining the corrected TG curve

the ignition behavior of the coal samples. The conversion degree (α) of a sample is defined by Eq. (1) [40]:

$$\alpha = \frac{m_0 - m_t}{m_0 - m_f} \tag{1}$$

where m_0 is the original mass of the sample, m_t is the mass at time t , and m_f is the final mass when the reaction stops.

The ignition behavior is characterized by the ignition temperature (T_i) and the peak temperature (T_p). T_i can be determined from the TG/DTG curves based on a commonly used method [41, 42] as follows. Point A in Fig. 4 shows the point at which a vertical line from the DTG peak (the maximum value in the DTG curve) meets the TG curve. Point B indicates the time when volatilization begins. The two lines that are tangent to the TG curve at A and B meet at point C, which corresponds to the ignition temperature. The temperature corresponding to point A, T_p ,

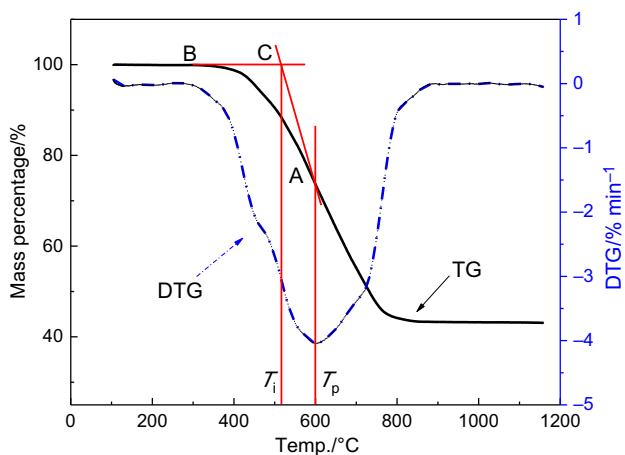


Fig. 4 Schematic of determining the ignition temperature (T_i) and the maximum mass losing rate temperature (T_p) from the TG/DTG profiles

is the temperature at which the maximum mass loss rate occurs on the DTG curve.

The activation energy is calculated using the Flynn–Wall–Ozawa (FWO) equation (Eq. 2) [27, 35, 43, 44]. It is widely used in the kinetic analysis of TG data.

$$\lg(\beta) = \lg\left(\frac{AE}{RG(\alpha)}\right) - 2.315 - 0.4567 \frac{E}{RT} \tag{2}$$

where β is the heating rate ($^{\circ}\text{C min}^{-1}$), $G(\alpha)$ is an integral form of the function depending on the reaction mechanism, T is the absolute temperature (K), E is the activation energy, and A is the pre-exponential factor.

For a given conversion degree, $G(\alpha)$ is considered constant. By plotting $\lg(\beta)$ versus $1/T$, the activation energy E can be related to the degree of conversion from the slopes of the linear fitting curves.

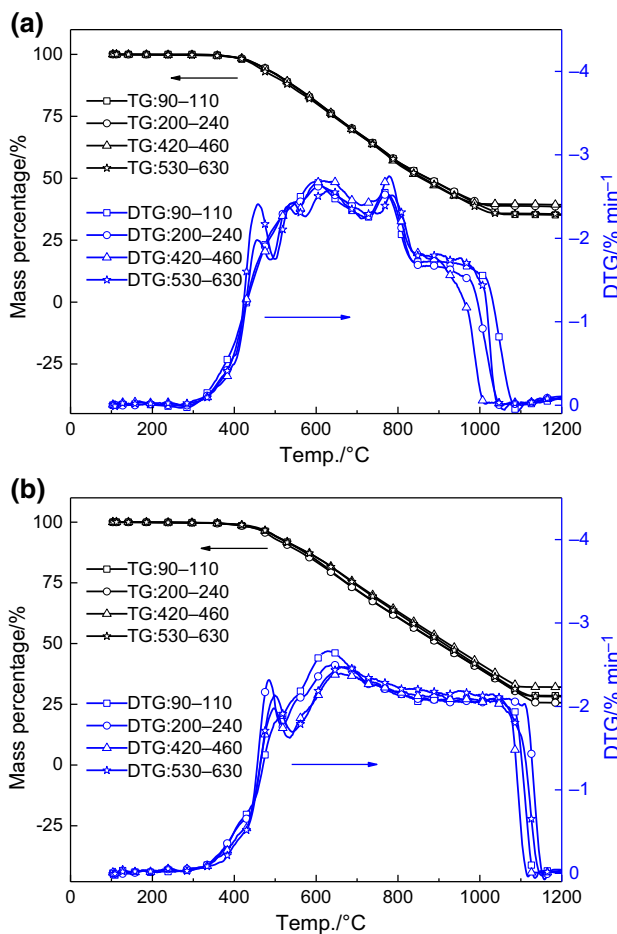


Fig. 5 TG and DTG curves of the DC (a) and the CZ (b) coals of four particle sizes at a heating rate of $20\text{ }^{\circ}\text{C min}^{-1}$ at an oxygen concentration of 6%

Results and discussion

Thermogravimetric analysis

Figure 5 shows the TG and DTG curves of the DC and CZ coals with different particle size distributions at a heating rate of $20\text{ }^{\circ}\text{C min}^{-1}$ and an oxygen concentration of 6%. Figure 6 shows the TG and DTG curves of the DC coal at heating rates of 10, 20, and $30\text{ }^{\circ}\text{C min}^{-1}$ with an oxygen concentration of 6%. Figure 7 shows the TG and DTG curves at oxygen concentrations of 3, 6, 9, and 12% and a heating rate of $20\text{ }^{\circ}\text{C min}^{-1}$.

The TG curves in Fig. 5 have almost the same trends for the different particle size distributions, and the particle size distribution has little influence on the shape of the TG/DTG curves for the same heating rate and oxygen concentration. The DTG curves of all samples exhibit three peaks, indicating that the combustion process can be divided into three steps. The first step is volatilization when the temperature was maintained at $104\text{ }^{\circ}\text{C}$ for 30 min. All the

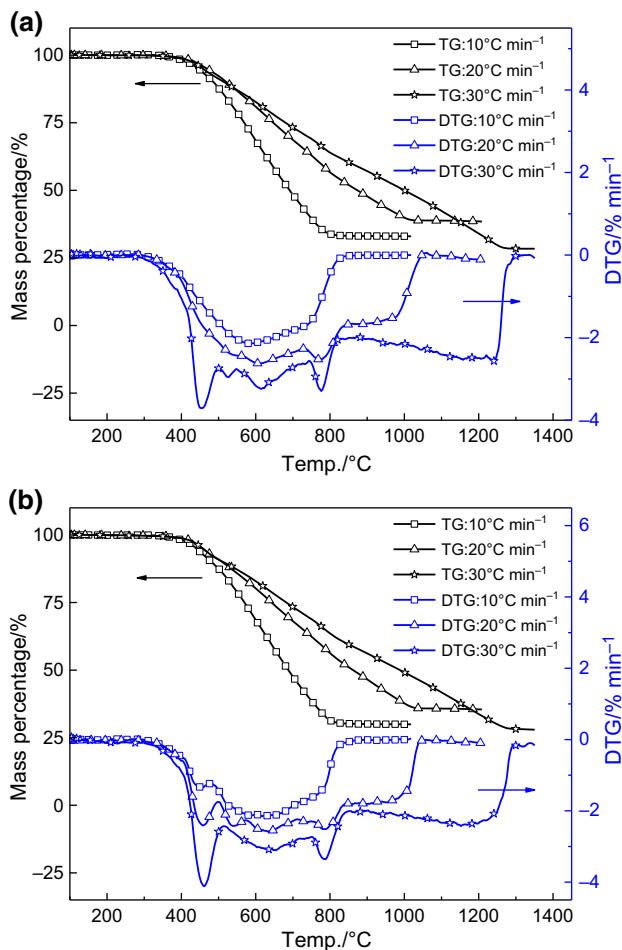


Fig. 6 TG and DTG curves of the DC coal at different heating rates at an oxygen concentration of 6%; **a** 200–240 μm , **b** 530–630 μm

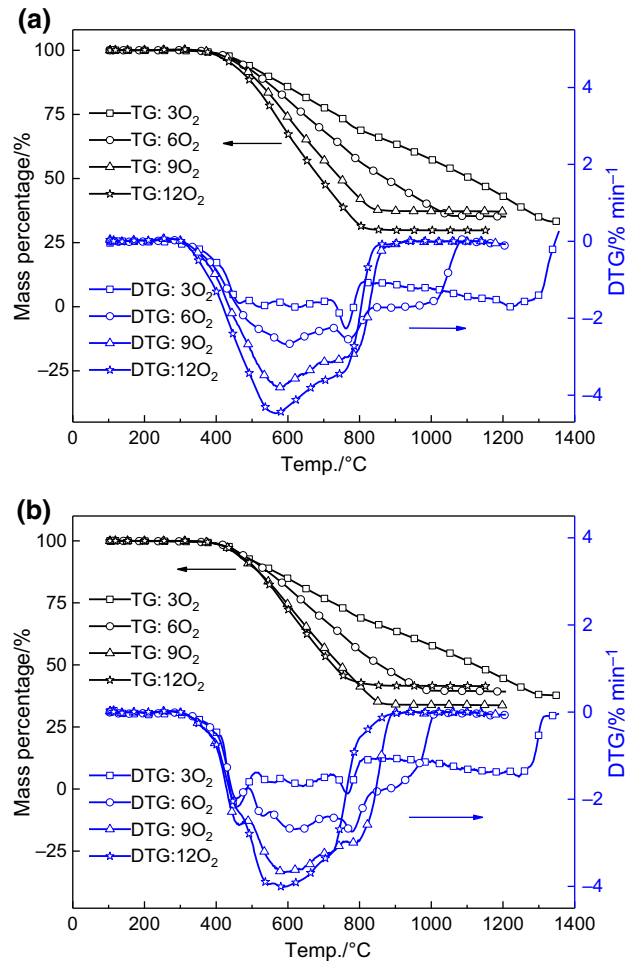


Fig. 7 TG and DTG curves of the DC coal at a heating rate of $20\text{ }^{\circ}\text{C min}^{-1}$ at different oxygen concentrations: **a** 90–110 μm , **b** 420–460 μm

moisture in the coal is removed, and the coal samples do not react with the oxygen because it was below the ignition temperature. The second step starts at $535\text{--}685\text{ }^{\circ}\text{C}$, depending on the oxygen concentration and heating rate, and it is characterized by a major mass loss. In this step, the volatile matter and fixed carbon are oxidized. The third step is char combustion.

A comparison between the DTG curves in Figs. 6 and 7 shows that the mass loss rate of the sample is expedited in the second step with increases in the heating rate and oxygen concentration, regardless of the particle size. In the first step, the heating rate has a clear positive correlation with the devolatilization rate. Similar patterns are not observed at the other oxygen concentrations, indicating that the devolatilization depends primarily on the temperature rather than the oxygen concentration. An increase in the heating rate improves the release of the volatile matter. The TG curves shift toward a low temperature with the increase

in the oxygen concentration, but this is not the case for the heating rate.

Effects of the oxygen concentration on the ignition temperature

Table 2 shows the characteristic parameters of the DC coal ignited at various oxygen concentrations. Figure 8 shows that the ignition temperature decreases with increasing oxygen concentration. As the oxygen concentration increases from 3 to 12%, the ignition temperatures of the DC coal decrease from 577, 585, 595, and 603 °C to 551, 559, 570, and 581 °C for the particle size ranges of 90–110, 200–240, 420–460, and 530–630 μm , respectively. The

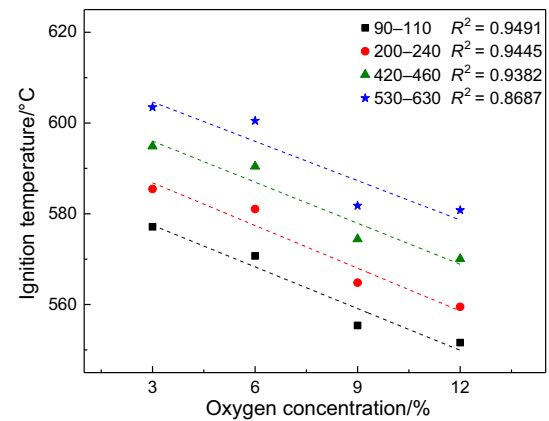


Fig. 8 Ignition temperature vs oxygen concentration for the DC coal at a heating rate of 20 °C min⁻¹

Table 2 Ignition parameters of the DC coal at a heating rate of 20 °C min⁻¹

Particle size distribution/ μm	Oxygen concentration/%	T_i /°C	T_p /°C	$(dm/dt)_{\text{max}}$ /% min ⁻¹
90–110	6 ^a	539.66	571.38	– 2.28
200–240		552.40	585.70	– 2.14
420–460		569.61	602.95	– 2.09
530–630		587.18	617.41	– 2.15
90–110	3 ^b	577.1	626.0	– 1.71
200–240		585.5	632.2	– 1.75
420–460		594.9	642.6	– 1.70
530–630		603.5	650.9	– 1.69
90–110	6 ^b	570.7	600.8	– 2.68
200–240		581.1	611.4	– 2.62
420–460		590.4	619.7	– 2.69
530–630		600.5	627.9	– 2.71
90–110	9 ^b	555.3	576.0	– 3.81
200–240		564.8	586.5	– 3.55
420–460		574.4	594.9	– 3.67
530–630		581.8	603.3	– 3.53
90–110	12 ^b	551.6	568.2	– 4.47
200–240		559.5	576.4	– 4.38
420–460		570.0	588.7	– 4.01
530–630		580.8	599.1	– 4.04
90–110	6 ^c	579.92	606.16	– 3.20
200–240		587.37	612.66	– 3.22
420–460		607.69	632.00	– 3.22
530–630		622.68	647.98	– 3.09
90–110	6 ^{b,d}	597.49	627.91	– 2.66
200–240		610.79	642.17	– 2.51
420–460		625.59	658.65	– 2.39
530–630		637.62	668.99	– 2.48

^a $\beta = 10$ °C min⁻¹

^b $\beta = 20$ °C min⁻¹

^c $\beta = 30$ °C min⁻¹

^dResults for CZ coal

respective maximum mass loss rates are 1.71, 2.68, 3.64, and 4.22.

Figure 7 shows that the duration of coal combustion is shortened when the oxygen concentration increases. The chemical reactions between the coal and oxygen proceed more quickly at a higher oxygen concentration. The ignition temperature decreases with the increase in the oxygen concentration, especially at concentrations of 6–9%, when the ignition temperatures drop rapidly. These results are not surprising because coal ignition represents the oxidation of the reactive substances in the coal. When the oxygen concentration is lower than 6%, the chemical reactions are deemed weak due to the limited amount of oxygen. When the oxygen concentration is higher than 9%, there is a sufficient oxygen supply and gaseous products are released, creating a barrier that limits the diffusion of oxygen. As a result, the intensity of the combustion slows down.

Figure 8 shows the linear correlation between the ignition temperature and the oxygen concentration. The ignition temperatures of all the samples decreased about 25 °C as the oxygen concentration increased from 3 to 12%. According to the linear regression equation, the ignition temperature decreases about 3 °C with a 1% increase in the oxygen concentration.

Effects of the heating rate on the ignition temperature

Figure 6a shows that, for the samples in the size range of 200–240 μm, there was only one mass loss peak in the DTG curve at the heating rate of 10 °C min⁻¹, whereas the DTG curves at 20 and 30 °C min⁻¹ show two and three peaks, respectively. This indicates that, to some extent, the chemical reactions also depend on the heating rate. Table 2 shows the ignition temperatures of the DC coal heated at three different rates at an oxygen concentration of 6%.

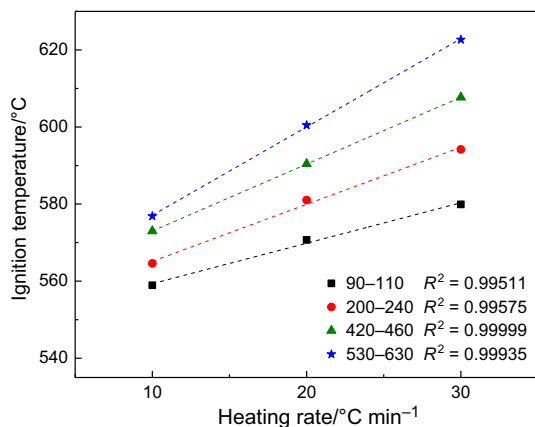


Fig. 9 Ignition temperatures at different heating rates for the DC coal at an oxygen concentration of 6%

Figure 9 shows the effects of the heating rate on the ignition temperature. There is a positive correlation between the heating rate and the ignition temperature. According to the linear regression results, the ignition temperature increases by about 2 °C when the heating rate increases from 10 to 30 °C min⁻¹.

The temperature profile within the coal particles is more uniform at a lower heating rate, and the combustion reactions proceed more adequately. The temperature gradient at the coal surface and the internal temperature of the coal particles increased with the increase in the heating rate and consequently enhanced devolatilization. However, subsequently, the temperature reached a higher level before the reaction stopped and weakened the out-diffusion of the gaseous products [31, 32]. On the other hand, in the same temperature range, a higher heating rate means a shorter

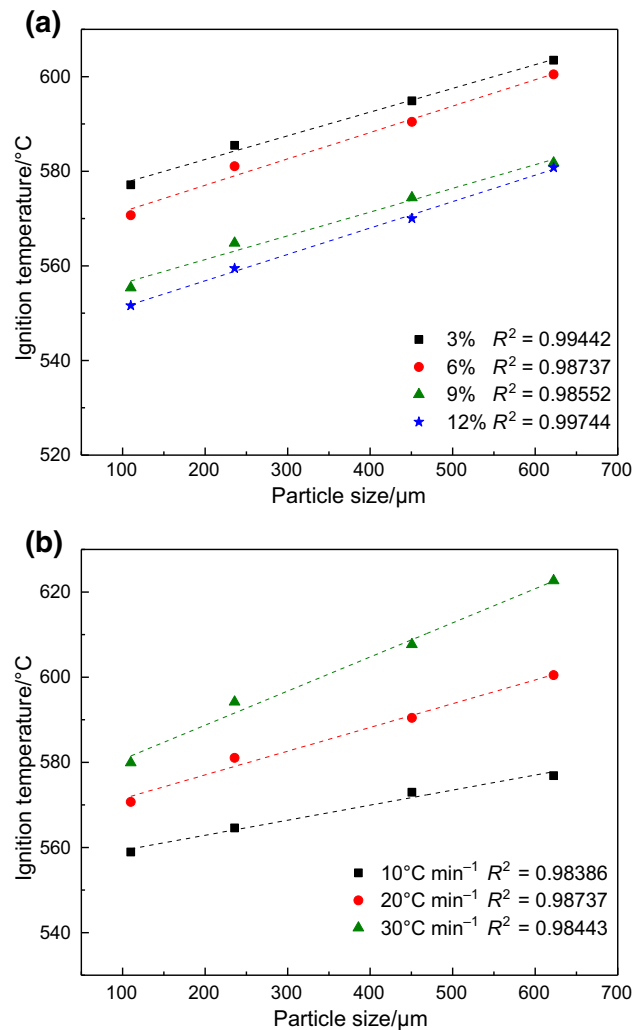


Fig. 10 Ignition temperatures of the DC coal samples with four particle sizes in different atmospheres: **a** different oxygen concentrations at a heating rate of 20 °C min⁻¹. **b** Different heating rates at an oxygen concentration of 6%

reaction time and a higher ignition temperature. In previous studies, the ignition of fuels was defined with respect to the type of reaction between the oxygen and the active substances; homogeneous and heterogeneous reactions occurred for gas–gas and gas–solid reactions, respectively [25, 45]. At a low heating rate, the ignition of low-rank coals is a homogeneous reaction for the combustion of volatile matter. At a high heating rate, the ignition is a heterogeneous reaction that is controlled to a greater degree by inter-particle diffusion.

Effects of the particle size on the ignition temperature

As shown in Fig. 10, all the DC coal samples, which were analyzed at the oxygen concentrations of 3, 6, 9, and 12% and at the heating rates of 10, 20, and 30 °C min⁻¹, showed positive correlations between the ignition temperatures and the respective particle sizes. The ignition

temperatures of the CZ coal samples listed in the last row of Table 2 also exhibited a similar trend, which indicates that the smaller coal particles were ignited more easily than the larger ones.

The ignition of coal particles is controlled by both the reaction kinetics and the diffusion of the reactants [25]. Our results can be attributed to the negative effects of the large particle size on the mass transfer of the reactants. The increased resistance to the mass transfer of the reactants to diffuse out of the particles may cause an increase in the ignition temperature. In addition, the actual internal temperature of a larger coal particle is lower than its surface temperature due to the thermal resistance; this slows down the volatilization of the particle and also reduces the gas yield during the coal ignition process. Figure 5 shows slight differences between the total mass loss in the TG curves and the value of the first peak in the DTG curves for the different particle sizes. The DTG peaks are more pronounced for the smaller particles. The ignition

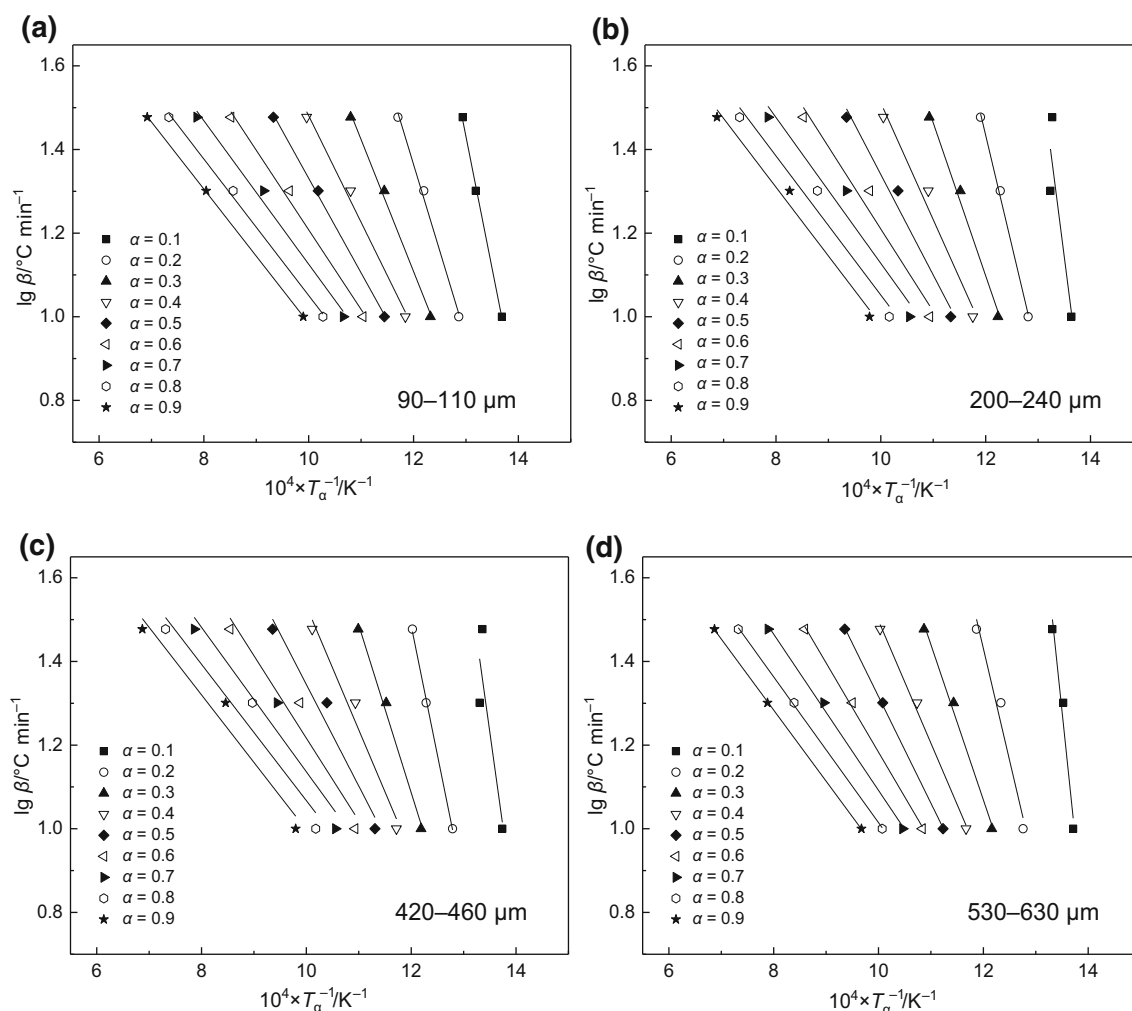


Fig. 11 Linear fitting for the activation energy using the FWO method

temperatures of the DC coal samples with a higher volatile content ($V_{\text{daf}} = 44.28\%$) are lower than those of the CZ coal samples with a lower volatile content (31.43%) (Table 2). This result confirmed the influence of the gas yield on the ignition temperature during coal combustion.

Analysis of kinetic parameters

The conversion degrees at each temperature were calculated using the TG results. As shown in Fig. 11, the activation energies were determined by the slope of the linear fitting curves of the plot of $\lg(\beta)$ versus $1/T$ for each conversion degree by using the FWO method at the three heating rates. The average activation energy values of the overall combustion reactions were 51.12, 62.57, 63.78, and 68.72 kJ mol^{-1} for the particle size ranges of 90–110, 200–240, 420–460, and 530–630 μm , respectively. The correlation coefficients of the fitting curves were all greater than 0.81.

Figure 12 shows the activation energy values at the conversion degrees ranging from 0.1 to 0.9 for different particle sizes. The activation energy values decrease rapidly during the early stage of the combustion process, and they vary greatly among the different particle sizes for conversion degrees of $\alpha < 0.4$. The average activation energy values are 82.58, 113.55, 116.51, and 127.75 kJ mol^{-1} for the four particle size ranges, respectively, at a conversion degree of less than 0.4. The corresponding ignition temperatures of the samples are 450–650 $^{\circ}\text{C}$. Subsequently, the activation energy values decrease slowly until the end of the combustion process and the differences in the activation energies of the different particle sizes are also narrow. The average values are 35.39, 37.07, 37.41, and 39.20 kJ mol^{-1} , respectively. This result was consistent with the previous findings that the

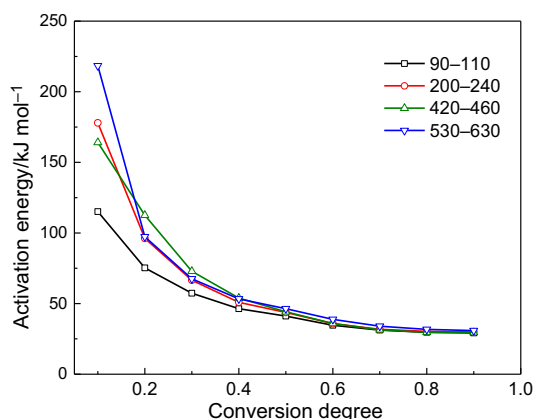


Fig. 12 Activation energy versus the conversion degree for the DC coal with different particle sizes at an oxygen concentration of 6%

reduction in the gas yield increased the activation energy of coal particles [29, 46, 47].

Conclusions

Two low-rank coals were characterized using TGA to understand the effects of oxygen concentration, particle size, and heating rate on the ignition temperature of the coal. The average activation energy values of the DC coal with four different particle sizes at an oxygen concentration of 6% were 51.12, 62.57, 63.78, and 68.72 kJ mol^{-1} from small to large, respectively. At an oxygen concentration in the range of 6–9%, the coal ignition temperature could be reduced by increasing the oxygen concentration. At an oxygen concentration greater than 9%, the influence weakened due to the increased resistance to the oxygen diffusion caused by a gaseous barrier surrounding the coal particles. The barrier was formed by an abundance of gaseous products with a sufficient oxygen supply. The ignition temperature decreased by about 25 $^{\circ}\text{C}$ as the oxygen concentration increased from 3 to 12%, but it increased slightly with an increase in the heating rate at the same oxygen concentrations. The mechanisms of coal ignition were attributed to the occurrence of a homogeneous reaction for the combustion of volatile matter at a low heating rate and a change into a heterogeneous reaction controlled by inter-particle diffusion at a high heating rate.

The activation energy varied greatly with the particle size at a conversion degree of less than 0.4. The particle size had a certain influence on the ignition temperature. The ignition temperature increased by about 8 $^{\circ}\text{C}$ with a 100- μm increase in the particle diameter at a heating rate of 10 $^{\circ}\text{C min}^{-1}$. The effects of the particle size on the ignition temperature were enhanced when the heating rate was 30 $^{\circ}\text{C min}^{-1}$. In addition, the coal with the higher volatile content (DC) had a lower ignition temperature. These results can be used by other researchers for process modeling and the design of CFB boilers with a graded particle size fuel-feed system.

Acknowledgements The financial support from the National Key R&D Program of China (Grant No. 2017YFB0603901) is gratefully acknowledged.

References

- Liu Y. China's carbon-emissions trading: overview, challenges and future. *Renew Sustain Energy Rev.* 2015;49:254–66.
- Xu WQ, Wan B, Zhu TY, Shao MP. CO₂ emissions from China's iron and steel industry. *J Clean Prod.* 2016;139:1504–11.
- Iftikhar Y, He W, Wang Z. Energy and CO₂ emissions efficiency of major economies: a non parametric analysis. *J Clean Prod.* 2016;139:779–87.

4. Anderson K. The trouble with negative emissions. *Science*. 2016;354(6309):182–3.
5. Nica E. Environmentally sustainable economic growth, energy use, and CO₂ emissions in China. *Econ Manag Financ Mark*. 2016;11(2):101–7.
6. Su T. The response of actual evaporation to global warming in China based on six reanalysis datasets. *Int J Climatol*. 2015;35(11):3238–48.
7. Yue G, Cai R, Lu J, Zhang H. From a CFB reactor to a CFB boiler—the review of R&D progress of CFB coal combustion technology in China. *Powder Technol*. 2017;316:18–28.
8. Shen B, Han Y, Price L, Lu H, Liu M. Techno-economic evaluation of strategies for addressing energy and environmental challenges of industrial boilers in China. *Energy*. 2017;118:526–33.
9. Yang H, Lu J, Zhang H, Yue G, Guo Y. Coal ignition characteristics in CFB boiler. *Fuel*. 2005;84(14):1849–53.
10. Kumar R, Singh RI. An investigation in 20 kWth oxygen-enriched bubbling fluidized bed combustor using coal and biomass. *Fuel Process Technol*. 2016;148(Supplement C):256–68.
11. Lit QH, Zhang YG, Meng AH. Design and application of novel horizontal circulating fluidized bed boiler. In: Yue G, Zhang H, Zhao C, Luo Z, editors. *Proceedings of the 20th international conference on fluidized bed combustion*. Berlin, Heidelberg: Springer; 2010. p. 206–11.
12. Heng F, Qinghai L, Meng A, Yanguo Z. A damköhler number for evaluating combustion efficiency of horizontal circulating fluidized bed boilers. In: Li J, Wei F, Bao X, Wang W, editors. *Proceedings of the 11th international conference on fluidized bed technology*. Beijing, China: Chemical Industry Press; 2014. p. 613–8.
13. Aihong M, Qinghai L, Yanguo Z, Zhaojun W, Wenda D. Experimental Investigation on a 0.35 MWth coal-fired horizontal circulating fluidized bed boiler. In: Qi H, Zhao B, editors. *Cleaner combustion and sustainable world*. Berlin, Heidelberg: Springer; 2013. p. 651–6.
14. Wang Q, Luo Z, Li X, Fang M, Ni M, Cen K. A mathematical model for a circulating fluidized bed (CFB) boiler. *Energy*. 1999;24(7):633–53.
15. Shi X, Lan X, Liu F, Zhang Y, Gao J. Effect of particle size distribution on hydrodynamics and solids back-mixing in CFB risers using CPFD simulation. *Powder Technol*. 2014;266(Supplement C):135–43.
16. Hultgren M, Ikonen E, Kovács J. Oxidant control and air-oxy switching concepts for CFB furnace operation. *Comput Chem Eng*. 2014;61(Supplement C):203–19.
17. Grotkjær T, Dam-Johansen K, Jensen AD, Glarborg P. An experimental study of biomass ignition. *Fuel*. 2003;82(7):825–33.
18. Arenillas A, Rubiera F, Arias B, Pis JJ, Faundez JM, Gordon AL, et al. A TG/DTA study on the effect of coal blending on ignition behaviour. *J Therm Anal Calorim*. 2004;76(2):603–14.
19. Avila I, Crnkovic PM, Luna CMR, Milioli FE. Use of a fluidized bed combustor and thermogravimetric analyzer for the study of coal ignition temperature. *Appl Therm Eng*. 2017;114:984–92.
20. Niu S, Chen M, Li Y, Lu T. Combustion characteristics of municipal sewage sludge with different initial moisture contents. *J Therm Anal Calorim*. 2017;129(2):1189–99.
21. Wang YF, Song YM, Zhi KD, Li Y, Teng YY, He RX, et al. Combustion kinetics of Chinese Shenhua raw coal and its pyrolysis carbocoal. *J Energy Inst*. 2017;90(4):624–33.
22. Lu JJ, Chen WH. Investigation on the ignition and burnout temperatures of bamboo and sugarcane bagasse by thermogravimetric analysis. *Appl Energy*. 2015;160:49–57.
23. Contreras ML, Garcia-Frutos FJ, Bahillo A. Study of the thermal behaviour of coal/biomass blends during oxy-fuel combustion by thermogravimetric analysis. *J Therm Anal Calorim*. 2016;123(2):1643–55.
24. Kosowska-Golachowska M. Thermal analysis and kinetics of coal during oxy-fuel combustion. *J Therm Sci*. 2017;26(4):355–61.
25. Magalhaes D, Kazanc F, Ferreira A, Rabacal M, Costa M. Ignition behavior of Turkish biomass and lignite fuels at low and high heating rates. *Fuel*. 2017;207:154–64.
26. Naktiyok J, Bayrakceken H, Ozer AK, Gulaboglu MS. Investigation of combustion kinetics of Umutbaca-lignite by thermal analysis technique. *J Therm Anal Calorim*. 2017;129(1):531–9.
27. Vyazovkin S, Chrissafis K, Di Lorenzo ML, Koga N, Pijolat M, Roduit B, et al. ICTAC kinetics committee recommendations for collecting experimental thermal analysis data for kinetic computations. *Thermochim Acta*. 2014;590:1–23.
28. Wang CB, Shao H, Lei M, Wu YH, Jia LF. Effect of the coupling action between volatiles, char and steam on isothermal combustion of coal char. *Appl Therm Eng*. 2016;93:438–45.
29. Li YL, Xing XJ, Xu BJ, Xing YQ, Zhang XF, Yang J, et al. Effect of the particle size on co-combustion of municipal solid waste and biomass briquette under N₂/O₂ and CO₂/O₂ atmospheres. *Energy Fuels*. 2017;31(1):932–40.
30. Shen J, Wang XS, Garcia-Perez M, Mourant D, Rhodes MJ, Li CZ. Effects of particle size on the fast pyrolysis of oil mallee woody biomass. *Fuel*. 2009;88(10):1810–7.
31. Bai FT, Sun YH, Liu YM. Thermogravimetric analysis of Huadian oil shale combustion at different oxygen concentrations. *Energy Fuels*. 2016;30(6):4450–6.
32. Qi X, Li Q, Zhang H, Xin H. Thermodynamic characteristics of coal reaction under low oxygen concentration conditions. *J Energy Inst*. 2017;90(4):544–55.
33. Bridgeman TG, Jones JM, Shield I, Williams PT. Torrefaction of reed canary grass, wheat straw and willow to enhance solid fuel qualities and combustion properties. *Fuel*. 2008;87(6):844–56.
34. Liu B, Zhang Z, Zhang H, Yang H, Zhang D. An experimental investigation on the effect of convection on the ignition behaviour of single coal particles under various O₂ concentrations. *Fuel*. 2014;116:77–83.
35. Jayaraman K, Gokalp I. Pyrolysis, combustion and gasification characteristics of miscanthus and sewage sludge. *Energy Conv Manag*. 2015;89:83–91.
36. Zhang L, Zou C, Wu D, Liu Y, Zheng CG. A study of coal chars combustion in O₂/H₂O mixtures by thermogravimetric analysis. *J Therm Anal Calorim*. 2016;126(2):995–1005.
37. Wang MY, Zhao R, Qing S, Liu YQ, Zhang AM. Study on combustion characteristics of young lignite in mixed O₂/CO₂ atmosphere. *Appl Therm Eng*. 2017;110:1240–6.
38. Moon C, Sung Y, Ahn S, Kim T, Choi G, Kim D. Thermochemical and combustion behaviors of coals of different ranks and their blends for pulverized-coal combustion. *Appl Therm Eng*. 2013;54(1):111–9.
39. Chao JN, Yang HR, Wu YX, Zhang H, Lv JF, Dong WG, et al. The investigation of the coal ignition temperature and ignition characteristics in an oxygen-enriched FBR. *Fuel*. 2016;183:351–8.
40. Yan L, He B, Hao T, Pei X, Li X, Wang C, et al. Thermogravimetric study on the pressurized hydrolysis kinetics of a lignite coal. *Int J Hydrogen Energy*. 2014;39(15):7826–33.
41. Li XG, Lv Y, Ma BG, Jian SW, Tan HB. Thermogravimetric investigation on co-combustion characteristics of tobacco residue and high-ash anthracite coal. *Biores Technol*. 2011;102(20):9783–7.
42. Liu Z, Quek A, Kent Hoekman S, Srinivasan MP, Balasubramanian R. Thermogravimetric investigation of hydrochar-lignite co-combustion. *Biores Technol*. 2012;123(Supplement C):646–52.

43. Niu S, Chen M, Li Y, Xue F. Evaluation on the oxy-fuel combustion behavior of dried sewage sludge. *Fuel*. 2016;178(Supplement C):129–38.
44. Cai JM, Wu WX, Liu RH. An overview of distributed activation energy model and its application in the pyrolysis of lignocellulosic biomass. *Renew Sustain Energy Rev*. 2014;36:236–46.
45. Yuan Y, Li S, Zhao F, Yao Q, Long MB. Characterization on hetero-homogeneous ignition of pulverized coal particle streams using CH₄ chemiluminescence and 3 color pyrometry. *Fuel*. 2016;184(Supplement C):1000–6.
46. Deng J, Li QW, Xiao Y, Wen H. The effect of oxygen concentration on the non-isothermal combustion of coal. *Thermochim Acta*. 2017;653:106–15.
47. Wang C, Zhang X, Liu Y, Che D. Pyrolysis and combustion characteristics of coals in oxyfuel combustion. *Appl Energy*. 2012;97:264–73.